

Article

# Controlling Plasmon Resonance of Gold and Silver Nanoparticle Arrays with Help of Liquid Crystal

Ivan Yakovkin <sup>1,\*</sup>  and Victor Reshetnyak <sup>1,2</sup> 

<sup>1</sup> Physics Faculty, Taras Shevchenko National University of Kyiv, 01601 Kyiv, Ukraine; victor.reshetnyak@knu.ua

<sup>2</sup> School of Physics and Astronomy, University of Leeds, Leeds LS2 9JT, UK

\* Correspondence: yakovkinii@gmail.com

**Abstract:** The tunability of plasmonic resonances in gold and silver nanosphere arrays on a glass substrate, embedded in a liquid crystal matrix, was explored. The calculations involving the finite element method revealed that the optical properties of these arrays can be modulated by reorienting the liquid crystal. When the liquid crystal director was reoriented between planar and homeotropic configurations in the plane containing the incident wave polarization vector, the plasmonic resonance wavelength shifted within an approximately 100 nm range. A reduced shift of about 40 nm was observed when the reorientation occurred in the plane perpendicular to the polarization. Both metal nanosphere arrays showed notable near-field amplification. Gold achieved up to 18 times the amplification of the incident wave electric field, while silver reached 16 times but showed a remarkable 40 times amplification at the inter-band transition resonance wavelength. This research underscores the potential of using liquid crystal reorientation for controlling the plasmonic lattice resonance in metal nanosphere arrays, opening up new possibilities for adaptable plasmonic devices.

**Keywords:** nanoparticle arrays; liquid crystals; plasmonic resonance tuning



**Citation:** Yakovkin, I.; Reshetnyak, V. Controlling Plasmon Resonance of Gold and Silver Nanoparticle Arrays with Help of Liquid Crystal.

*Photonics* **2023**, *10*, 1088. <https://doi.org/10.3390/photonics10101088>

Received: 31 August 2023

Revised: 23 September 2023

Accepted: 27 September 2023

Published: 28 September 2023



**Copyright:** © 2023 by the authors. Licensee MDPI, Basel, Switzerland. This article is an open access article distributed under the terms and conditions of the Creative Commons Attribution (CC BY) license (<https://creativecommons.org/licenses/by/4.0/>).

## 1. Introduction

The ordered arrangement of nanoparticles into periodic arrays over large areas is an important requirement to obtain functional interfaces for real-life applications. When plasmonic nanostructures are arranged periodically, the electrodynamic coupling of the nanostructures enhances the light–matter interaction compared to isolated nanostructures due to localized surface plasmon resonances (LSPRs) and surface lattice resonances (SLR) [1,2].

The applications of these plasmonic nanostructure arrays are manifold. They have been demonstrated for light-harvesting enhancement in photovoltaic applications [3–5], utilized in photocatalytic processes [6,7], and employed in photothermal-mediated processes [8,9]. Additionally, the pronounced near-field enhancement due to plasmonic coupling in these arrays has facilitated advancements in spectroscopic techniques. This includes improvements in surface-enhanced Raman spectroscopy [10–12] and fluorescence [13,14]. Recent reports have also shown potential in surface-enhanced infrared absorption spectroscopy [15,16] and in photoemission and photodetection signals [17]. The fabrication of these nanoparticle arrays necessitates precision. Self-assembly emerges as a promising technique, offering a straightforward and cost-effective approach to producing periodic arrays of nanoparticles [18,19]. By leveraging the nanoparticles as foundational building blocks, it becomes feasible to engineer arrays with functionalities tailored for specific applications [20,21]. Over recent years, there has been a growing interest in self-assembled films of nanoparticles, both in terms of their fabrication methodologies and their emergent applications [22,23].

One of the important features of self-assembly is the granular control it affords over various parameters. This encompasses the packing configuration, interparticle gap, and

the number of layers [24]. Such control is crucial for customizing the arrays for specific applications. For instance, self-assembled plasmonic nanoparticle films, especially those comprising gold, have shown potential for sensing applications due to their increased sensitivity to the local dielectric environment [25,26].

A long-standing goal in plasmonics and cavity photonics has been the active modulation of cavity resonances by adjusting external parameters. The surface plasmon resonance maximum is very sensitive to the dielectric constant of the surrounding media [27–29]. The large anisotropy of the liquid crystal (LC) refractive index is therefore ideally suited for tuning the plasmon resonance by an electric-field-induced switching of the liquid crystal director orientation.

The potential of LCs to actively modulate resonances in metallic nanostructures has been previously demonstrated in various contexts, including single nanoparticles [30–33], thin metallic films [34–36], metallic hole arrays [37,38], metasurfaces [39–47], and metallic nanoparticle arrays [48–52]. The reported resonance shifts due to liquid crystal director reorientation are within a 10–100 nm range and significantly depend on the specific structure studied. Specifically, in [32], the authors reported the tunability of individual gold nanorods with liquid crystals of up to 30 nm, while an exceptional 100% scattering modulation for single nanoparticles was reported in [33]. The tunability of a 2D rectangular nanohole array by using a thermal transition of liquid crystal was demonstrated in [37], with up to a 40 nm shift in the wavelength of the plasmonic resonance. The authors in [46] reported a 75% transmission modulation of a 2D rectangular silicon nanodisc array through liquid crystal reorientation. The spontaneous emission of a 2D rectangular silicon nanodisc array placed on a fluorescent glass substrate was shown to be tunable within a 20 nm range in [47]. In [48], the hexagonal nanodot array was shown to be tunable within a 10 nm wavelength range.

Notably, in [49], a 1D array of metallic nanospheres was semi-analytically studied to show that the geometric resonance in such a structure can be significantly controlled within 100 nm. This control range can potentially be increased even further by utilizing liquid crystals with very high birefringence due to the linear dependence of the control range on the interparticle distance and the birefringence. In [52], up to a 24 nm control range was achieved by studying the 2D arrays of gold cylinders for the E7 liquid crystal. While other methods for creating tunable metasurfaces exist, such as using phase change materials or electrical gating [53–57], LCs stand out due to their cost-effectiveness, ease of integration, and minimal optical losses.

In this work, we investigate the potential for the dynamic tunability of self-assembled 2D gold and silver nanosphere arrays using LCs. A shift in plasmonic resonance wavelength of up to 100 nm is observed as a result of changing the LC orientation for both gold and silver nanospheres. Such plasmonic resonance tunability holds promise for the development of adjustable lasers and enhanced plasmonic sensors.

## 2. Structure Description

In this article, dynamic control and tunability are introduced to the properties of the metallic nanosphere arrays, as reported in [58,59], by incorporating a liquid crystal, as depicted in Figure 1. The structure begins with a semi-infinite glass substrate with a refractive index  $n_{\text{glass}} = 1.5$ . Directly on top of the substrate are metallic nanospheres, self-assembled to form a 2D hexagonal structure. We consider the cases of gold and silver nanospheres with a diameter  $d = 10$  nm and an inter-particle gap of  $g = 2$  nm. The refractive indexes of gold and silver were taken from [60].

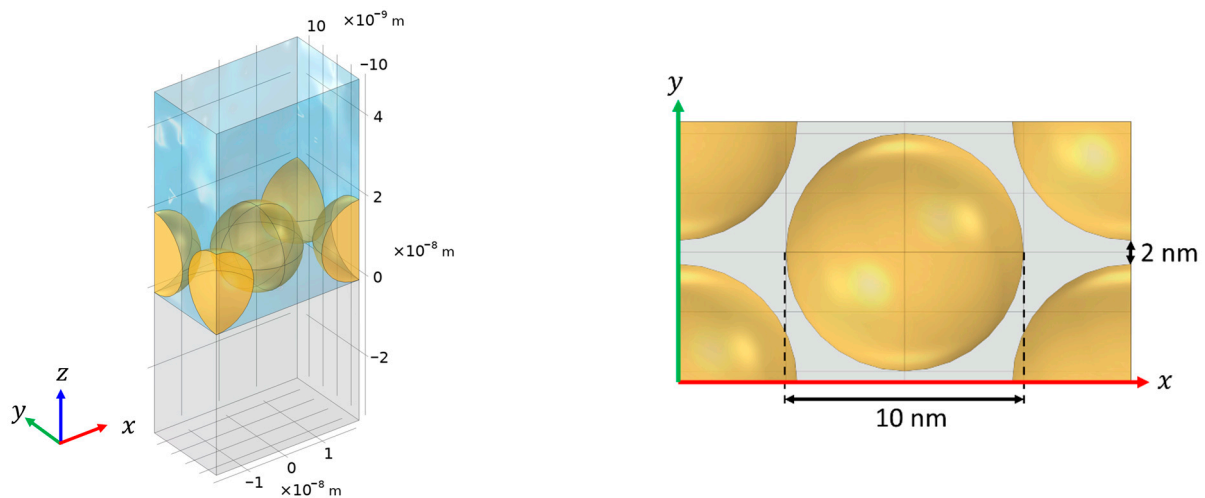


**Figure 1.** Unit cell of the structure under study (left panel) and its dimensions (right panel).

The space above the nanospheres is filled with a liquid crystal, which, for simplicity, is considered to be semi-infinite in the  $z$  direction. The ordinary and extraordinary refractive indices of LC were chosen to be  $n_o = 1.7$  and  $n_e = 2.2$ , respectively, corresponding to the high-birefringence LC mixtures reported in [61,62].

In order to showcase the potential extent of tuning the properties of nanoparticle arrays through liquid crystal reorientation, we performed a comparison of the transmittance, absorbance, and reflectance spectra of such nanoparticle arrays for the three principal LC director orientations: along the  $z$  axis (homeotropic), along the  $x$ -axis (further denoted as ‘planar  $x$ ’), and along the  $y$ -axis (‘planar  $y$ ’). The calculations were performed for the  $x$ - and  $y$ -polarized normally incident plane waves. While the boundary conditions can sometimes prevent the LC from reorienting at the substrate, full reorientation can be achieved using a photoalignment layer [63].

### 3. Materials and Methods

The calculations were performed using the finite element method in COMSOL Multiphysics. The structure was represented by a unit cell, as depicted on Figure 1. The dimensions of the unit cell were set to  $12\sqrt{3}$  by 12 nm in order to produce the hexagonal arrangement of the nanospheres. The incident wave was excited using a periodic port. The Floquet periodic boundary conditions were applied at the  $x$ - and  $y$ -boundaries of the cell, with the Floquet vector being derived from the periodic port. The semi-infinite span of the substrate and LC in the  $z$  direction was modelled by using cartesian perfectly matched layers.

The reflectance and transmittance spectra were calculated by integrating the normal Poynting component at the upper and lower boundaries, and the absorbance spectra by integrating the resistive losses over the volume of the unit cell. The mesh was adapted to reflect the peculiarities of the structure, such as accounting for a finer resolution needed near the areas of near-field enhancement, the symmetry requirements for the mesh in the perfectly matched layers for correct domain stretching, and the results were verified to be stable with respect to mesh adjustments. The described approach was extensively verified to produce correct results in the cases where analytical solutions are available, and multiple sanity checks were performed on the obtained data. The validity of the numerical results was additionally cross-checked by performing a separate calculation using the scattered-field formulation and by matching the results reported in [58,59] without the liquid crystal.

## 4. Results

### 4.1. Optical Spectra for the Gold Nanoparticle Array

The periodic structure of the gold nanoparticle array results in the excitation of the plasmonic lattice resonance. Figure 2 shows the reflectance, transmittance, and absorbance spectra for the gold nanoparticle array for the x-polarized incident plane wave. A broad resonance peak is clearly visible in the reflectance spectrum at around 710 nm in the case of a homeotropic liquid crystal orientation, reaching a value of 0.8 with a full width at half maximum of approximately 300 nm. The transmittance spectrum shows a matching dip for this resonance, while the absorbance varies monotonically.

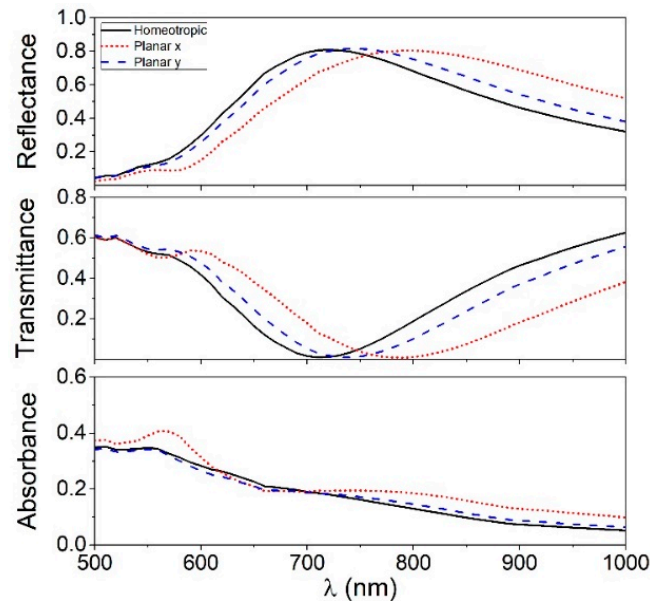


**Figure 2.** Reflectance (**top**), transmittance (**middle**), and absorbance (**bottom**) of hexagonal gold nanoparticle array for homeotropic and two planar LC orientations for x-polarized incident light.

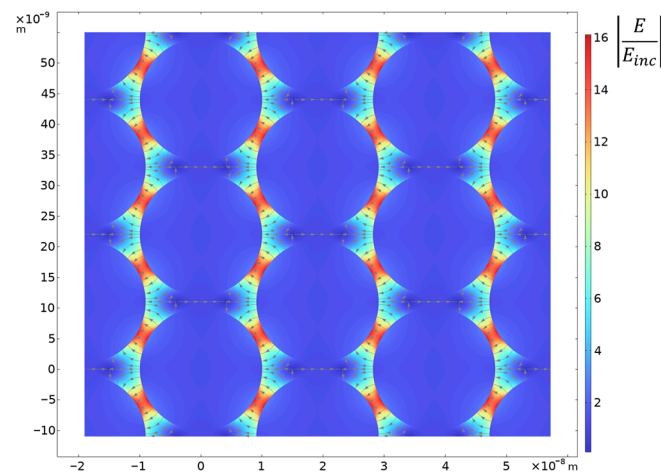
When the liquid crystal director is reoriented, which could be achieved in multiple ways, for example, by applying an in-plane electric field, through photo-orientation [64,65], or using a magnetic field, the refractive index tensor changes near the areas where the resonance is localized, therefore shifting its wavelength. Since the incident light polarization is along the x-direction, the electric field taking part in the lattice resonance consists mostly of its x-component. This makes the resonance sensitive to the reorientation of the director in the x–z plane, which maximizes the change in the respective refractive index component.

The reorientation of the liquid crystal director in the x–z plane results in a shift of the resonance wavelength toward larger values by approximately 100 nm. This shift is manifested as the shifts of the respective peaks of the reflectance and transmittance spectra. The overall shape of the reflectance and transmittance spectra remain intact, and the peak reflectance value remains constant at a level of 0.8. The absorbance spectrum remains qualitatively unchanged during the reorientation of the director of the liquid crystal, with only a slight gradual increase by less than 0.1 in the long-wave region.

When the director is being reoriented in the y–z plane, the effect of the reorientation on the plasmonic resonance remains, although it is substantially weaker. The overall shift of the transmission and reflection resonance peaks is reduced to approximately 40 nm. That is, the effect of liquid crystal director reorientation in the y–z plane is around 2.5 times weaker compared to that in the x–z plane. The absorption spectrum remains qualitatively unchanged, similarly to the case of director reorientation in the x–z plane, and is nearly identical to the absorbance spectrum for the case of homeotropic liquid crystal orientation.

The existence of the effect of liquid crystal director reorientation in the y–z plane on the plasmonic resonance in the case of x-polarized incident light can be explained by the

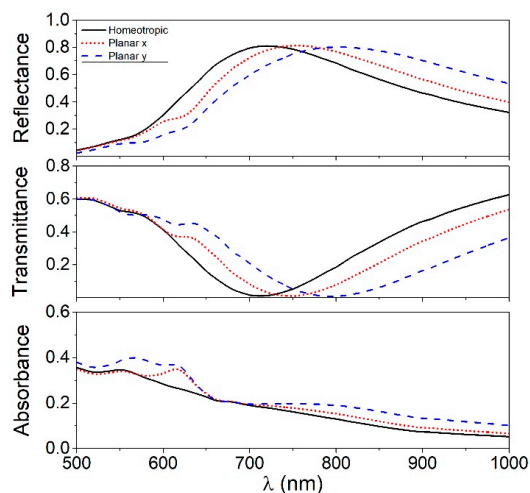
involvement of multiple electric field components in the resonance, making it sensitive to all components of the refractive index tensor. This becomes apparent upon examination of the electric field distribution at the resonance frequency. Figure 3 shows the distribution of the electric field norm in the plane  $z = R$  at the resonance wavelength of 700 nm for the case of homeotropic liquid crystal orientation. The color represents the electric field norm relative to that of the incident wave, and the arrows show the direction of the electric field vector between the nanospheres. The electric field is almost completely concentrated in the areas where the nanospheres are the closest to each other. It should be noted that despite the structure being symmetric with respect to the rotations by an angle of 60 degrees, the electric field norm distribution is lacking the maxima where the nanospheres contact in the  $y$ -direction. This is due to the fact that the initial wave polarization is along the  $x$ -direction, and due to the reflection symmetry in the  $y$ -direction, such maxima cannot occur. The lines of the electric field show that the electric field in the distribution maxima has both  $x$ - and  $y$ -components, meaning that such structure introduces a  $y$ -component of the electric field, making it sensitive to the director reorientation in the  $y$ - $z$  plane.



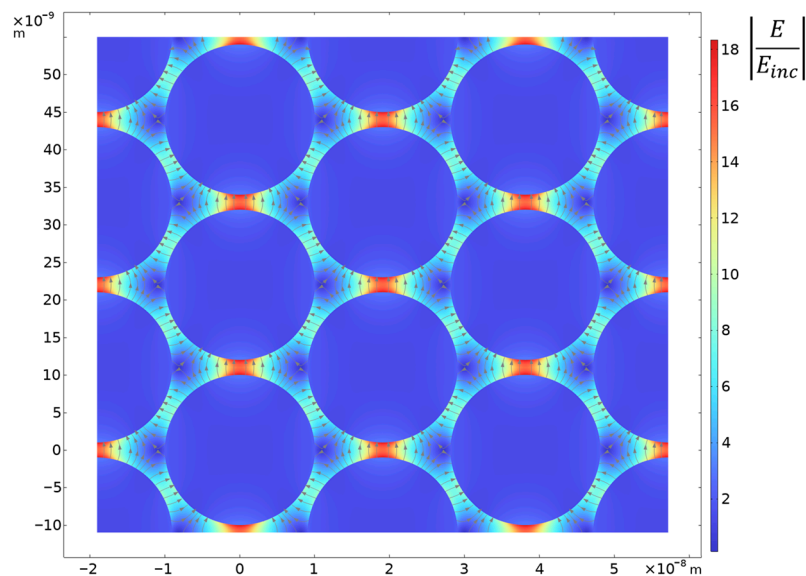
**Figure 3.** Electric field norm distribution corresponding to the 710 nm plasmonic resonance for homeotropic liquid crystal director orientation and  $x$ -polarization.

Figure 4 shows the reflectance, transmittance, and absorbance spectra for the case of  $y$ -polarized incident wave. The overall shape of the reflectance, transmittance, and absorbance spectra is very similar to the case of an  $x$ -polarized incident wave described above. The major difference is that for the  $y$ -polarized incident light, the liquid crystal director reorientation in the  $x$ - $z$  plane becomes the most efficient for shifting the resonance wavelength. The magnitude of the resonance wavelength shift is similar to the case of  $x$ -polarized incident light, being around 40 nm for the liquid crystal director reorientation in the  $x$ - $z$  plane and approximately 100 nm for that in the  $y$ - $z$  plane.

Figure 5 shows the electric field norm distribution for a homeotropic liquid crystal director orientation with the incident light polarized along the  $y$ -axis. The distribution is qualitatively different from the case of  $x$ -polarization (Figure 3), where some resonances were missing due to symmetry. In the case of the  $y$ -polarized incident wave, the electric field norm has maxima in all the proximity areas, and the maximums between the nanospheres in the  $y$ -directions are dominant in this case. The existence of angled maxima makes the structure sensitive to the director reorientation in the  $x$ - $z$  plane, both qualitatively and quantitatively, similar to the mechanism in the case of an  $x$ -polarized incident wave. In summary, introducing the liquid crystal to the structure with a nanoparticle array does allow for a gradual control of the plasmonic resonance wavelength without distorting the transmittance, reflectance and absorbance profile shapes, and such control persists irrespective of the incident wave polarization and the director reorientation plane.



**Figure 4.** Reflectance (top), transmittance (middle), and absorbance (bottom) of hexagonal gold nanosphere array for homeotropic and two planar LC orientations for y-polarized incident light.



**Figure 5.** Electric field norm distribution corresponding to the 710 nm plasmonic resonance for homeotropically aligned liquid crystal director orientation and y-polarization.

*4.2. Optical Spectra for the Silver Nanoparticle Array*

Silver nanoparticle arrays can manifest similar plasmonic resonances to gold nanoparticle arrays. However, silver has inter-band transitions that are in the visible range [66], resulting in complex features appearing in reflectance, transmittance, and absorbance. The calculation of these spectra for the silver nanospheres in the case of an x-polarized incident wave is presented in Figure 6.

The shape of the reflectance, transmittance, and absorbance spectra can be attributed to two separate effects. In the 500–800 nm area, the gradual reflectance peak has the same origin as the resonance in the gold nanoparticle array described in the previous section. It can be characterized by a smooth and gradual reflectance peak, the matching transmittance dip, and monotonic absorbance profile. The electric field norm distribution is similar to the corresponding case of gold nanospheres, with the electric field being localized in the gaps between the nanospheres (Figure 7).

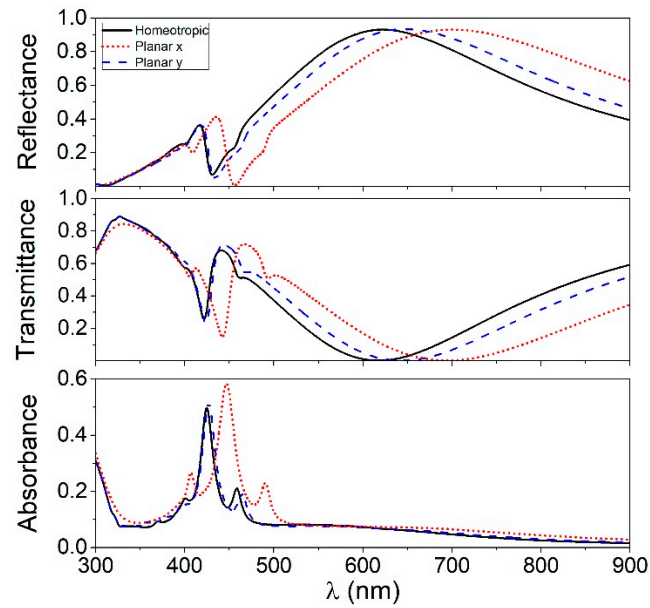


**Figure 6.** Reflectance (**top**), transmittance (**middle**), and absorbance (**bottom**) of hexagonal silver nanosphere array for homeotropic and two planar LC orientations for x-polarized incident light.

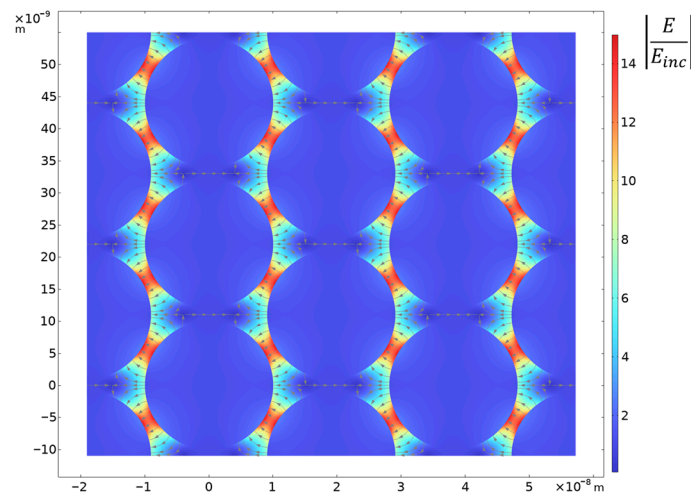


**Figure 7.** Electric field norm distribution corresponding to the 625 nm plasmonic resonance for the case of homeotropically aligned liquid crystal director orientation and x-polarization.

The other effect taking place is to be attributed to the inter-band transitions and is manifested as well-pronounced absorbance peaks below 500 nm, with corresponding reflectance and transmittance dips. It can also be noted that the reflectance dips are slightly shifted toward higher wavelength than the corresponding transmittance dips. The electric field distribution for the peak of 425 nm is shown in Figure 8 and is qualitatively different, with the electric field maxima being near the surface of the nanospheres and partially penetrating inside the nanoparticles.

When the liquid crystal director is reoriented from the homeotropic to the planar state in the  $x$ - $z$  plane, both resonances are shifted toward higher wavelengths. The plasmonic band resonance shifts by approximately 100 nm, while the resonance associated with the inter-band transitions is shifted much less, by about 30 nm. Similar to the case of gold nanospheres, the reorientation of the liquid crystal director in the  $y$ - $z$  plane corresponds to an approximately 2.5-times-weaker effect for the  $x$ -polarized incident wave.

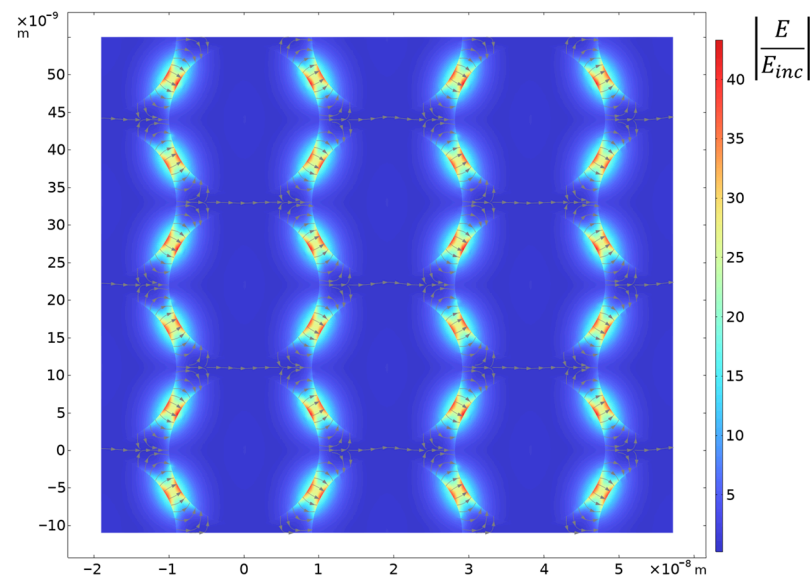


**Figure 8.** Electric field norm distribution at a wavelength of 425 nm plasmonic resonance corresponding to the inter-band transitions in the case of homeotropically aligned liquid crystal director orientation and x-polarization.

The case of a y-polarized incident wave is generally in line with the pattern observed for gold nanospheres: changing the polarization has only a little effect on the general shape of the reflectance, transmittance, and absorbance spectra, making the director reorientation in the y–z plane more efficient for resonance wavelength control (Figures 9 and 10). It is worth noting that, contrary to the case with an x-polarized incident wave, the reorientation of the liquid crystal director results in a significant intensity redistribution between the peaks related to the inter-band transitions, resulting in two distinct peaks at 450 and 510 nm, respectively.

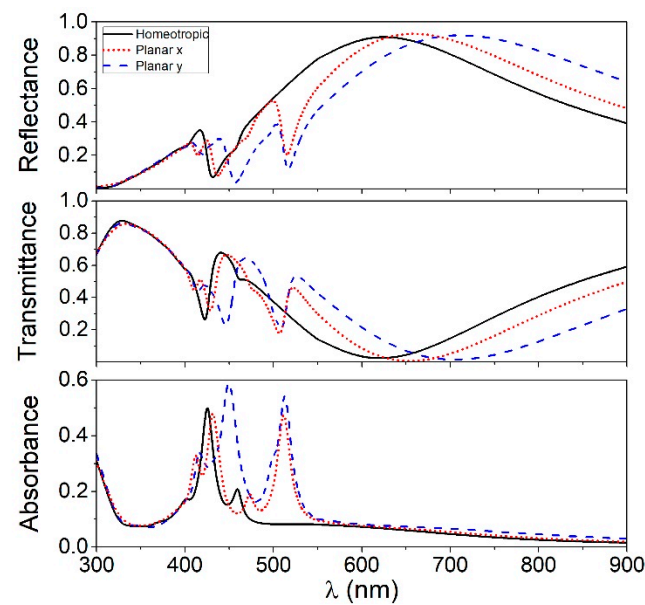


**Figure 9.** Reflectance (top), transmittance (middle), and absorbance (bottom) of hexagonal silver nanosphere array for homeotropic and two planar LC orientations for y-polarized incident light.

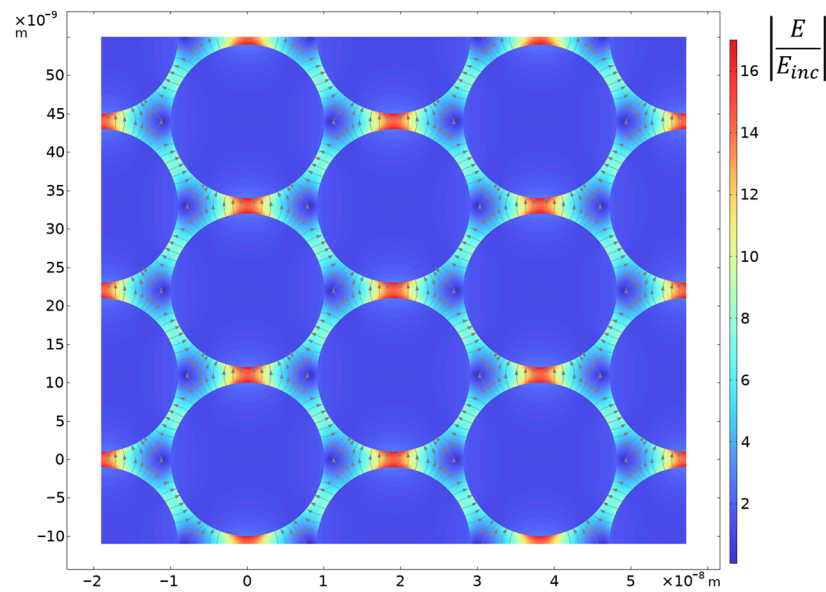


**Figure 10.** Electric field norm distribution corresponding to the 620 nm plasmonic resonance for the case of homeotropically aligned liquid crystal director orientation and y-polarization.

### 5. Discussion

The obtained plasmonic resonance tuning range for both the silver and gold nanoparticle arrays reaches a value of  $\Delta\lambda \approx 100$  nm, which is a relatively high tunability for such structures. While the localized surface plasmon resonances are quite broad, the tuning range reaches more than one third of its full width at half maximum. Intensity-wise, the available control reaches 20–30% in the transmittance and reflectance, and it should be noted that increasing the birefringence of the liquid crystal will likely increase this range even more, especially considering the recent reports of liquid crystals with an extremely high birefringence of up to  $\Delta n = 0.8$  [61,62].

While the current work focuses on numeric simulations, it can be quite convenient to have some analytic expressions to estimate the tunability range for such structures. The latter can be achieved by using the framework developed in [67], specifically through equation from the mentioned work. This equation allows the sensitivity,  $S = \delta\lambda/\delta n$ , of the resonance peak wavelength to the changes in the refractive index to be estimated as a function of the geometric factor,  $\Gamma$ , the liquid crystal mean refractive index,  $n_{LC}$ , the peak wavelength,  $\lambda$ , and the  $\epsilon_\infty$  parameter from the Drude model fit of the dielectric function of the metal nanoparticles. For the liquid crystal used in the calculations, we take the average refractive index of the liquid crystal to be equal to  $n_{LC} = 1.95$ , while for spherical nanoparticles,  $\Gamma$  takes a value of one third. The  $\epsilon_\infty$  parameter allows us to conveniently take into account the difference between silver and gold nanoparticles. For gold, the Drude model fit for the visible range leads to  $\epsilon_\infty$  values around 11 [68], while for silver, this value is around 5 [69]. The substitution of these values leads to  $S \approx 160$  nm/RIU for the 750 nm resonance for gold, and around 200 nm/RIU for the 650 nm silver resonance, where RIU stands for refractive index units. Substituting the birefringence of the liquid crystal of  $\Delta n = 0.5$ , we obtain  $\Delta\lambda \approx 80$  nm and  $\Delta\lambda \approx 100$  nm for gold and silver, respectively, which turns out to be a very reasonable estimate. Therefore, the approach presented in [67] is likely applicable for providing quick estimates on how the tunability would change when using a liquid crystal with slightly different dielectric properties.

It is notable that such a broad control range was obtained for the localized surface plasmon resonances, which are known to often have a relatively limited tunability. For comparison, the extended surface plasmonic resonances (surface plasmon polaritons) can have a tunability higher by several orders of magnitude [70], which makes introducing the coupling of the localized resonances in studied structures with the extended surface plas-

mon resonances [71] a promising avenue for further research. It is also worth mentioning the role of the 2 nm gap between the nanoparticles considered in the presented simulations. The presence of such a gap leads to the nanospheres being disconnected so that there is no electrical current flowing between the nanoparticles. Contact between the nanospheres would lead to the whole array acting as a single conductor, which would conversely reflect in the modes excited. The presence of such a gap between the nanoparticles and its influence on the plasmonic resonances were studied in detail in [72,73]. These works have shown that the exact size of the gap has a significant and non-linear impact on the interaction of such nanoparticles with the incident wave. Therefore, changing the inter-particle gap leads to significant changes in the electric field amplification, as well as the nanoparticle size and other structural details for the optimal excitation of the plasmonic resonance.

While we consider a complete director reorientation throughout the entire liquid crystal, the boundary conditions can often prevent such a complete reorientation. If the liquid crystal is not fully reoriented near the nanoparticles, the impact of such reorientation on the plasmonic resonances would significantly diminish, since the resonance peak wavelength is most sensitive to the dielectric function in the areas with the highest electric field amplification. Without any special treatment, the experimentally observed control range would likely be significantly reduced. However, covering the nanoparticles with an alignment layer and using photo-orientation techniques [63–65] were shown to help enforce the desired orientation at the boundaries.

The tunable nature of plasmonic resonances in metal nanoparticle arrays, facilitated by liquid crystal reorientation, opens up a range of prospective applications. The foremost is tunable sensing: the ability to modify the resonant frequency based on environmental factors could lead to more adaptable sensors. This tunability also hints at potential innovations in optoelectronic devices, where precise control over resonance can enable more efficient modulators or switches. Overall, the essence of the presented design's value lies in its adaptability, offering flexible and precise control over light–matter interactions.

## 6. Conclusions

The tunability of plasmonic resonances in closely packed gold and silver nanosphere arrays embedded in a liquid crystal matrix was studied. The optical properties were shown to be controllable by reorienting the liquid crystal, leading to a shift in the plasmon frequency and thus affecting the transmittance, reflectance, and absorbance spectra.

The reorientation of the liquid crystal director between planar and homeotropic configurations in the plane containing the incident wave polarization vector was shown to be most effective for controlling the plasmonic resonance wavelength, allowing for shifting it within an approximately 100 nm range, signifying the potential for dynamic tunability in LSPR-based devices. The reorientation of the director in the plane perpendicular to the incident wave polarization also impacted the resonance wavelength in a reduced range of approximately 40 nm.

Silver nanosphere arrays have shown more complex transmittance, reflectance, and absorbance spectra due to the peaks related to the inter-band transitions in the 400–500 nm wavelength range. A liquid crystal director reorientation from the homeotropic to the planar states increased the wavelength of such peaks, although to a lower extent, and in the case of *y*-polarized incident light, led to a significant redistribution of the peak intensities.

Both the silver and gold nanosphere arrays demonstrated significant near-field amplification. Gold nanospheres had a slightly stronger amplification of up to around 18 times the incident wave electric field, compared to a 16-times amplification for silver. However, the silver nanospheres had a significantly higher amplification of up to 40 times at the wavelength corresponding to the inter-band transition resonance.

Overall, our results highlight the possibility of using liquid crystal reorientation to control LSPRs in metal nanosphere arrays, contributing to the development of tunable and reconfigurable plasmonic devices.

**Author Contributions:** Conceptualization, I.Y. and V.R.; methodology, V.R.; software, I.Y. and V.R.; validation, I.Y. and V.R.; formal analysis, I.Y. and V.R.; investigation, I.Y. and V.R.; writing—original draft preparation, I.Y.; writing—review and editing, I.Y. and V.R.; visualization, I.Y.; supervision, V.R.; All authors have read and agreed to the published version of the manuscript.

**Funding:** This research received no external funding.

**Institutional Review Board Statement:** Not applicable.

**Informed Consent Statement:** Not applicable.

**Data Availability Statement:** Data underlying the results presented in this paper are not publicly available at this time but may be obtained from the authors upon reasonable request.

**Conflicts of Interest:** The authors declare no conflict of interest.

## References

1. Kravets, V.G.; Kabashin, A.V.; Barnes, W.L.; Grigorenko, A.N. Plasmonic surface lattice resonances: A review of properties and applications. *Chem. Rev.* **2018**, *118*, 5912–5951. [[CrossRef](#)] [[PubMed](#)]
2. Borah, R.; Verbruggen, S.W. Coupled plasmon modes in 2d gold nanoparticle clusters and their effect on local temperature control. *J. Phys. Chem. C* **2019**, *123*, 30594–30603. [[CrossRef](#)]
3. Bi, Y.-G.; Feng, J.; Ji, J.-H.; Yi, F.-S.; Li, Y.-F.; Liu, Y.-F.; Zhang, X.-L.; Sun, H.-B. Nanostructures induced light harvesting enhancement in organic photovoltaics. *Nanophotonics* **2017**, *7*, 371–391. [[CrossRef](#)]
4. Stratakis, E.; Kymakis, E. Nanoparticle-based plasmonic organic photovoltaic devices. *Mater. Today* **2013**, *16*, 133–146. [[CrossRef](#)]
5. Ou, Q.-D.; Xie, H.-J.; Chen, J.-D.; Zhou, L.; Li, Y.-Q.; Tang, J.-X. Enhanced light harvesting in flexible polymer solar cells: Synergistic simulation of a plasmonic meta-mirror and a transparent silver mesowire electrode. *J. Mater. Chem. A* **2016**, *4*, 18952–18962. [[CrossRef](#)]
6. Lim, S.Y.; Law, C.S.; Bertó-Roselló, F.; Liu, L.; Markovic, M.; Ferré-Borrull, J.; Abell, A.D.; Voelcker, N.H.; Marsal, L.F.; Santos, A. Tailor-engineered plasmonic single-lattices: Harnessing localized surface plasmon resonances for visible-NIR light-enhanced photocatalysis. *Catal. Sci. Technol.* **2020**, *10*, 3195–3211. [[CrossRef](#)]
7. Li, S.; Miao, P.; Zhang, Y.; Wu, J.; Zhang, B.; Du, Y.; Han, X.; Sun, J.; Xu, P. Recent advances in plasmonic nanostructures for enhanced photocatalysis and electrocatalysis. *Adv. Mater.* **2021**, *33*, e2000086. [[CrossRef](#)]
8. Song, L.; Qiu, N.; Huang, Y.; Cheng, Q.; Yang, Y.; Lin, H.; Su, F.; Chen, T. Macroscopic orientational gold nanorods monolayer film with excellent photothermal anticounterfeiting performance. *Adv. Opt. Mater.* **2020**, *8*, 1902082. [[CrossRef](#)]
9. Lin, K.-T.; Lin, H.; Jia, B. Plasmonic nanostructures in photodetection, energy conversion and beyond. *Nanophotonics* **2020**, *9*, 3135–3163. [[CrossRef](#)]
10. Wang, H.; Yao, L.; Mao, X.; Wang, K.; Zhu, L.; Zhu, J. Gold nanoparticle superlattice monolayer with tunable interparticle gap for surface-enhanced Raman spectroscopy. *Nanoscale* **2019**, *11*, 13917–13923. [[CrossRef](#)]
11. Bai, S.; Hu, A.; Hu, Y.; Ma, Y.; Obata, K.; Sugioka, K. Plasmonic superstructure arrays fabricated by laser near-field reduction for wide-range sers analysis of fluorescent materials. *Nanomaterials* **2022**, *12*, 970. [[CrossRef](#)]
12. Su, D.; Yang, S.; Xiong, Y.; Yang, X.; Yu, X.; Zeng, P.; Wu, Y.; Cheng, Y.; Zhang, T.; Shen, H.; et al. Ordered Gold Nanocluster-Based Plasmonic Hotspot Arrays for SERS Detection of Single Molecules. *ACS Appl. Nano Mater.* **2022**, *5*, 17067–17077. [[CrossRef](#)]
13. Pang, J.S.; Theodorou, I.G.; Centeno, A.; Petrov, P.K.; Alford, N.M.; Ryan, M.P.; Xie, F. Tunable Three-Dimensional Plasmonic Arrays for Large Near-Infrared Fluorescence Enhancement. *ACS Appl. Mater. Interfaces* **2019**, *11*, 23083–23092. [[CrossRef](#)]
14. Saito, T.; Takahashi, S.; Obara, T.; Itabashi, N.; Imai, K. Platinum plasmonic nanostructure arrays for massively parallel single-molecule detection based on enhanced fluorescence measurements. *Nanotechnology* **2011**, *22*, 445708. [[CrossRef](#)]
15. Mayerhöfer, T.G.; Popp, J. Periodic array-based substrates for surface-enhanced infrared spectroscopy. *Nanophotonics* **2018**, *7*, 39–79. [[CrossRef](#)]
16. Yang, X.; Sun, Z.; Low, T.; Hu, H.; Guo, X.; García de Abajo, F.J.; Avouris, P.; Dai, Q. Nanomaterial-based plasmon-enhanced infrared spectroscopy. *Adv. Mater.* **2018**, *30*, 1704896. [[CrossRef](#)]
17. Piltan, S.; Sievenpiper, D. Plasmonic nano-arrays for enhanced photoemission and photodetection. *J. Opt. Soc. Am. B* **2018**, *35*, 208–213. [[CrossRef](#)]
18. Fleischer, K.; Ualibek, O.; Verre, R.; Shvets, I.V. Formation of plasmonic nanoparticle arrays -rules and recipes for an ordered growth. *Phys. Status Solidi (B)* **2016**, *253*, 198–205. [[CrossRef](#)]
19. Gao, B.; Arya, G.; Tao, A.R. Self-orienting nanocubes for the assembly of plasmonic nanojunctions. *Nat. Nanotechnol.* **2012**, *7*, 433–437. [[CrossRef](#)]
20. Angioletti-Uberti, S. Theory, simulations and the design of functionalized nanoparticles for biomedical applications: A Soft Matter Perspective. *npj Comput. Mater.* **2017**, *3*, 48. [[CrossRef](#)]
21. Lin, J.X.; Hu, H.W.; Luo, J.; Miao, L.; Yang, Z.H.; Chen, M.; Zhang, M.; Ou, J.Z. Micro/nanoarrays and their applications in flexible sensors: A review. *Mater. Today Nano* **2022**, *19*, 100224. [[CrossRef](#)]

22. Mühlig, S.; Cunningham, A.; Dintinger, J.; Scharf, T.; Bürgi, T.; Lederer, F.; Rockstuhl, C. Self-assembled plasmonic metamaterials. *Nanophotonics* **2013**, *2*, 211–240. [[CrossRef](#)]
23. Conti, Y.; Passarelli, N.; Mendoza-Carreño, J.; Scarabelli, L.; Mihi, A. Colloidal Silver Nanoparticle Plasmonic Arrays for Versatile Lasing Architectures via Template-Assisted Self-Assembly. *Adv. Opt. Mater.* **2023**, 2300983. [[CrossRef](#)]
24. Rastogi, R.; Beggiato, M.; Adam, P.M.; Juodkazis, S.; Krishnamoorthy, S. Nanoplasmonic Arrays with High Spatial Resolutions, Quality, and Throughput for Quantitative Detection of Molecular Analytes. In *Nanoplasmonics*; IntechOpen: London, UK, 2019.
25. Hwang, Y.; Ferhan, A.R.; Yoon, B.K.; Sut, T.N.; Jeon, W.-Y.; Koo, D.J.; Jackman, J.A.; Cho, N.-J. Surface engineering of plasmonic gold nanoisland platforms for high-sensitivity refractometric biosensing applications. *Appl. Mater. Today* **2022**, *26*, 101280. [[CrossRef](#)]
26. Tay, L.-L.; Hulse, J. Self-Assembled Plasmonic Array Sensors for Cannabinoids. In *Optical Sensors*; Optica Publishing Group: Washington, DC, USA, 2022; p. SM4E-6.
27. Ghosh, S.K.; Nath, S.; Kundu, S.; Esumi, K.; Pal, T. Solvent and Ligand Effects on the Localized Surface Plasmon Resonance (LSPR) of Gold Colloids. *J. Phys. Chem. B* **2004**, *108*, 13963–13971. [[CrossRef](#)]
28. Templeton, A.C.; Pietron, J.J.; Murray, R.W.; Mulvaney, P. Solvent refractive index and core charge influences on the surface plasmon absorbance of alkanethiolate monolayer-protected gold clusters. *J. Phys. Chem. B* **2000**, *104*, 564–570. [[CrossRef](#)]
29. Underwood, S.; Mulvaney, P. Effect of the Solution Refractive Index on the Color of Gold Colloids. *Langmuir* **1994**, *10*, 3427–3430. [[CrossRef](#)]
30. Chu, K.C.; Chao, C.Y.; Chen, Y.F.; Wu, Y.C.; Chen, C.C. Electrically controlled surface plasmon resonance frequency of gold nanorods. *Appl. Phys. Lett.* **2006**, *89*, 2335812. [[CrossRef](#)]
31. Evans, P.R.; Wurtz, G.A.; Hendren, W.R.; Atkinson, R.; Dickson, W.; Zayats, A.V.; Pollard, R.J. Electrically switchable nonreciprocal transmission of plasmonic nanorods with liquid crystal. *Appl. Phys. Lett.* **2007**, *91*, 043101. [[CrossRef](#)]
32. Müller, J.; Sönnichsen, C.; von Poschinger, H.; von Plessen, G.; Klar, T.A.; Feldmann, J. Electrically controlled light scattering with single metal nanoparticles. *Appl. Phys. Lett.* **2002**, *81*, 171–173. [[CrossRef](#)]
33. Khatua, S.; Chang, W.-S.; Swanglap, P.; Olson, J.; Link, S. Active Modulation of Nanorod Plasmons. *Nano Lett.* **2011**, *11*, 3797–3802. [[CrossRef](#)]
34. Wang, Y. Voltage-induced color-selective absorption with surface plasmons. *Appl. Phys. Lett.* **1995**, *67*, 2759–2761. [[CrossRef](#)]
35. Wang, Y.; Russell, S.D.; Shimabukuro, R.L. Voltage-induced broad-spectrum reflectivity change with surface-plasmon waves. *Journal of applied physics* **2005**, *97*, 023708. [[CrossRef](#)]
36. Li, H.; Xu, S.; Gu, Y.; Wang, K.; Xu, W. Active modulation of wavelength and radiation direction of fluorescence via liquid crystal-tuned surface plasmons. *Appl. Phys. Lett.* **2013**, *102*, 051107. [[CrossRef](#)]
37. Cetin, A.E.; Mertiri, A.; Huang, M.; Erramilli, S.; Altug, H. Thermal Tuning of Surface Plasmon Polaritons Using Liquid Crystals. *Adv. Opt. Mater.* **2013**, *1*, 915–920. [[CrossRef](#)]
38. Dickson, W.; Wurtz, G.A.; Evans, P.R.; Pollard, R.J.; Zayats, A.V. Electronically controlled surface plasmon dispersion and optical transmission through metallic hole arrays using liquid crystal. *Nano Lett.* **2008**, *8*, 281–286. [[CrossRef](#)]
39. Dolan, J.A.; Cai, H.; Delalande, L.; Li, X.; Martinson, A.B.F.; de Pablo, J.J.; López, D.; Nealey, P.F. Broadband Liquid Crystal Tunable Metasurfaces in the Visible: Liquid Crystal Inhomogeneities Across the Metasurface Parameter Space. *ACS Photonics* **2021**, *8*, 567–575. [[CrossRef](#)]
40. Decker, M.; Kremers, C.; Minovich, A.; Staude, I.; Miroshnichenko, A.E.; Chigrin, D.; Neshev, D.N.; Jagadish, C.; Kivshar, Y.S. Electro-optical switching by liquid-crystal controlled metasurfaces. *Opt. Express* **2013**, *21*, 8879–8885. [[CrossRef](#)]
41. Zou, C.; Amaya, C.; Fasold, S.; Muravsky, A.A.; Murauski, A.A.; Pertsch, T.; Staude, I. Multiresponsive Dielectric Metasurfaces. *ACS Photonics* **2021**, *8*, 1775–1783. [[CrossRef](#)]
42. Kowrdziej, R.; Wróbel, J.; Kula, P. Ultrafast electrical switching of nanostructured metadvice with dual-frequency liquid crystal. *Sci. Rep.* **2019**, *9*, 20367. [[CrossRef](#)]
43. Xiao, S.; Chettiar, U.K.; Kildishev, A.V.; Drachev, V.; Khoo, I.C.; Shalae, V.M. Tunable magnetic response of metamaterials. *Appl. Phys. Lett.* **2009**, *95*, 033115. [[CrossRef](#)]
44. Komar, A.; Fang, Z.; Bohn, J.; Sautter, J.; Decker, M.; Miroshnichenko, A.; Pertsch, T.; Brener, I.; Kivshar, Y.S.; Staude, I.; et al. Electrically tunable all-dielectric optical metasurfaces based on liquid crystals. *Appl. Phys. Lett.* **2017**, *110*, 071109. [[CrossRef](#)]
45. Zou, C.; Komar, A.; Fasold, S.; Bohn, J.; Muravsky, A.A.; Murauski, A.A.; Pertsch, T.; Neshev, D.N.; Staude, I. Electrically Tunable Transparent Displays for Visible Light Based on Dielectric Metasurfaces. *ACS Photonics* **2019**, *6*, 1533–1540. [[CrossRef](#)]
46. Sautter, J.; Staude, I.; Decker, M.; Rusak, E.; Neshev, D.N.; Brener, I.; Kivshar, Y.S. Active Tuning of All-Dielectric Metasurfaces. *ACS Nano* **2015**, *9*, 4308–4315. [[CrossRef](#)]
47. Bohn, J.; Bucher, T.; Chong, K.E.; Komar, A.; Choi, D.-Y.; Neshev, D.N.; Kivshar, Y.S.; Pertsch, T.; Staude, I. Active Tuning of Spontaneous Emission by Mie-Resonant Dielectric Metasurfaces. *Nano Lett.* **2018**, *18*, 3461–3465. [[CrossRef](#)]
48. Kossyrev, P.A.; Yin, A.; Cloutier, S.G.; Cardimona, D.A.; Huang, D.; Alsing, P.M.; Xu, J.M. Electric Field Tuning of Plasmonic Response of Nanodot Array in Liquid Crystal Matrix. *Nano Lett.* **2005**, *5*, 1978–1981. [[CrossRef](#)]
49. Li, J.; Ma, Y.; Gu, Y.; Khoo, I.-C.; Gong, Q. Large spectral tunability of narrow geometric resonances of periodic arrays of metallic nanoparticles in a nematic liquid crystal. *Appl. Phys. Lett.* **2011**, *98*, 3592756. [[CrossRef](#)]

50. Abass, A.; Rodriguez, S.R.-K.; Ako, T.; Aubert, T.; Verschuuren, M.; Van Thourhout, D.; Beeckman, J.; Hens, Z.; Rivas, J.G.; Maes, B. Active Liquid Crystal Tuning of Metallic Nanoantenna Enhanced Light Emission from Colloidal Quantum Dots. *Nano Lett.* **2014**, *14*, 5555–5560. [[CrossRef](#)]
51. van Heijst, E.A.P.; ter Huurne, S.E.T.; Sol, J.A.H.P.; Castellanos, G.W.; Ramezani, M.; Murai, S.; Debije, M.G.; Rivas, J.G. Electric tuning and switching of the resonant response of nanoparticle arrays with liquid crystals. *J. Appl. Phys.* **2022**, *131*, 083101. [[CrossRef](#)]
52. Dridi, M.; Vial, A. Modeling of metallic nanostructures embedded in liquid crystals: Application to the tuning of their plasmon resonance. *Opt. Lett.* **2009**, *34*, 2652–2654. [[CrossRef](#)]
53. Ee, H.-S.; Agarwal, R. Tunable Metasurface and Flat Optical Zoom Lens on a Stretchable Substrate. *Nano Lett.* **2016**, *16*, 2818–2823. [[CrossRef](#)] [[PubMed](#)]
54. Zhang, X.; Zhou, Y.; Zheng, H.; Linares, A.E.; Ugwu, F.C.; Li, D.; Sun, H.-B.; Bai, B.; Valentine, J.G. Reconfigurable Metasurface for Image Processing. *Nano Lett.* **2021**, *21*, 8715–8722. [[CrossRef](#)] [[PubMed](#)]
55. Ding, F.; Yang, Y.; Bozhevolnyi, S.I. Dynamic Metasurfaces Using Phase-Change Chalcogenides. *Adv. Opt. Mater.* **2019**, *7*, 1801709. [[CrossRef](#)]
56. Yao, Y.; Shankar, R.; Kats, M.A.; Song, Y.; Kong, J.; Loncar, M.; Capasso, F. Electrically Tunable Metasurface Perfect Absorbers for Ultrathin Mid-Infrared Optical Modulators. *Nano Lett.* **2014**, *14*, 6526–6532. [[CrossRef](#)]
57. Huang, Y.-W.; Lee, H.W.H.; Sokhoyan, R.; Pala, R.A.; Thyagarajan, K.; Han, S.; Tsai, D.P.; Atwater, H.A. Gate-Tunable Conducting Oxide Metasurfaces. *Nano Lett.* **2016**, *16*, 5319–5325. [[CrossRef](#)]
58. Borah, R.; Ninakanti, R.; Bals, S.; Verbruggen, S.W. Plasmon resonance of gold and silver nanoparticle arrays in the Kretschmann (attenuated total reflectance) vs. direct incidence configuration. *Sci. Rep.* **2022**, *12*, 15738. [[CrossRef](#)]
59. Borah, R.; Smets, J.; Ninakanti, R.; Tietze, M.L.; Ameloot, R.; Chigrin, D.N.; Bals, S.; Lenaerts, S.; Verbruggen, S.W. Self-Assembled Ligand-Capped Plasmonic Au Nanoparticle Films in the Kretschmann Configuration for Sensing of Volatile Organic Compounds. *ACS Appl. Nano Mater.* **2022**, *5*, 11494–11505. [[CrossRef](#)]
60. Johnson, P.B.; Christy, R.W. Optical Constants of the Noble Metals. *Phys. Rev. B* **1972**, *6*, 4370. [[CrossRef](#)]
61. Arakawa, Y.; Kang, S.; Tsuji, H.; Watanabe, J.; Konishi, G.-I. The design of liquid crystalline bistolane-based materials with extremely high birefringence. *RSC Adv.* **2016**, *6*, 92845–92851. [[CrossRef](#)]
62. Dąbrowski, R.; Kula, P.; Herman, J. High Birefringence Liquid Crystals. *Crystals* **2013**, *3*, 443–482. [[CrossRef](#)]
63. Palermo, G.; Cataldi, U.; De Sio, L.; Bürgi, T.; Tabiryani, N.; Umeton, C. Optical control of plasmonic heating effects using reversible photo-alignment of nematic liquid crystals. *Appl. Phys. Lett.* **2016**, *109*, 191906. [[CrossRef](#)]
64. Yaroshchuk, O.; Reznikov, Y. Photoalignment of liquid crystals: Basics and current trends. *J. Mater. Chem.* **2012**, *22*, 286–300. [[CrossRef](#)]
65. Hirankittiwong, P.; Chattham, N.; Limtrakul, J.; Haba, O.; Yonetake, K.; Eremin, A.; Stannarius, R.; Takezoe, H. Optical manipulation of the nematic director field around microspheres covered with an azo-dendrimer monolayer. *Opt. Express* **2014**, *22*, 20087–20093. [[CrossRef](#)] [[PubMed](#)]
66. Kolwas, K.; Derkachova, A. Impact of the Interband Transitions in Gold and Silver on the Dynamics of Propagating and Localized Surface Plasmons. *Nanomaterials* **2020**, *10*, 1411. [[CrossRef](#)] [[PubMed](#)]
67. Abdulhalim, I. Liquid crystal active nanophotonics and plasmonics: From science to devices. *J. Nanophotonics* **2012**, *6*, 061001. [[CrossRef](#)]
68. Alabastri, A.; Tuccio, S.; Giugni, A.; Toma, A.; Liberale, C.; Das, G.; De Angelis, F.; Di Fabrizio, E.; Zaccaria, R.P. Molding of Plasmonic Resonances in Metallic Nanostructures: Dependence of the Non-Linear Electric Permittivity on System Size and Temperature. *Materials* **2013**, *6*, 4879–4910. [[CrossRef](#)]
69. Yang, H.U.; D’Archangel, J.; Sundheimer, M.L.; Tucker, E.; Boreman, G.D.; Raschke, M.B. Optical dielectric function of silver. *Phys. Rev. B* **2015**, *91*, 235137. [[CrossRef](#)]
70. Abdulhalim, I. Surface plasmon TE and TM waves at the anisotropic film–metal interface. *J. Opt. A: Pure Appl. Opt.* **2008**, *11*, 015002. [[CrossRef](#)]
71. Abdulhalim, I. Coupling configurations between extended surface electromagnetic waves and localized surface plasmons for ultrahigh field enhancement. *Nanophotonics* **2018**, *7*, 1891–1916. [[CrossRef](#)]
72. Li, A.; Isaacs, S.; Abdulhalim, I.; Li, S. Ultrahigh Enhancement of Electromagnetic Fields by Exciting Localized with Extended Surface Plasmons. *J. Phys. Chem. C* **2015**, *119*, 19382–19389. [[CrossRef](#)]
73. Li, A.; Srivastava, S.K.; Abdulhalim, I.; Li, S. Engineering the hot spots in squared arrays of gold nanoparticles on a silver film. *Nanoscale* **2016**, *8*, 15658–15664. [[CrossRef](#)] [[PubMed](#)]

**Disclaimer/Publisher’s Note:** The statements, opinions and data contained in all publications are solely those of the individual author(s) and contributor(s) and not of MDPI and/or the editor(s). MDPI and/or the editor(s) disclaim responsibility for any injury to people or property resulting from any ideas, methods, instructions or products referred to in the content.